Korean J. Chem. Eng., 39(3), 461-474 (2022)
DOI: 10.1007/s11814-021-1009-8

pISSN: 0256-1115
eISSN: 1975-7220

INVITED REVIEW PAPER

Recent progress in electrochemical reduction of CO_2 into formate and C_2 compounds

Wei Jyun Wang*, Louis Scudiero,†, and Su Ha*,†**

*The Gene and Linda Voiland School of Chemical Engineering and Bioengineering, Washington State University, Wegner Hall Room 105, 1505, NE Stadium Way, Pullman, WA 99164
**Chemistry Department and Materials Science and Engineering Program, Washington State University, PO Box 644630, Pullman, WA 99164-4630

(*Received 13 September 2021 • Revised 29 October 2021 • Accepted 10 November 2021*)

Abstract−Global warming and climate change enhanced by the high atmospheric CO_2 concentration have been correlated to the frequency of extreme weather causing a significant amount of property damage and loss of human lives. Among current atmospheric CO_2 concentration control strategies, the electrochemical reduction of CO_2 (eCO_2R) process is a promising technology that can utilize CO_2 gas as a feedstock to produce valuable C_1 and C_2 compounds at room temperature. Since the eCO_2R reaction is limited by high activation energy and mass transfer, the choice of the electrocatalyst and the configuration of the CO_2 electrolyzer have a significant impact on the activity and selectivity of the eCO_2R process. This review discusses current technological advancements of electrocatalytic materials and the design of the gas diffusion electrodes that increase energy efficiency and reduce the mass transfer resistance of the CO_2 conversion into C_1 with a focus on formate and C_2 chemical compounds. A techno-economic analysis is briefly provided, and future and technical challenges of the CO_2 conversion at the industrial scale into formate and C_2 products are also addressed.

Keywords: Electrochemical Reduction, Carbon Dioxides, Electrolyzer, Formate, C2 Compounds

INTRODUCTION

1. Impact of Global Warming and Climate Change on Human Society

Since the first industrial revolution in the 18th century, energy consumption worldwide from fossil fuel has produced an enormous amount of carbon dioxide (CO_2). Fig. 1 shows the average CO_2 concentration in the atmosphere for the past 800,000 years. In 2018, the global average atmospheric CO_2 concentration reached 407.4 ppm, which is 1.36 times more than the highest level observed in the past one million years [1,2]. The high amount of atmospheric CO_2 in the atmosphere further enhances the greenhouse effect and global warming, which is linked to the increase in the frequency of catastrophic storms and to the rising sea levels. In 2017, Hurricane Harvey brought in an estimated 65 to 70 inches of precipitation to southern Texas causing $125 billion in damage [3,4]. In the same year, Florida and Puerto Rico were struck by Hurricane Irma and Hurricane Maria, respectively, causing an additional $141 billion in damage [5,6]. Moreover, the continuous rise of the sea level is predicted to cause residential areas with 300 million people to

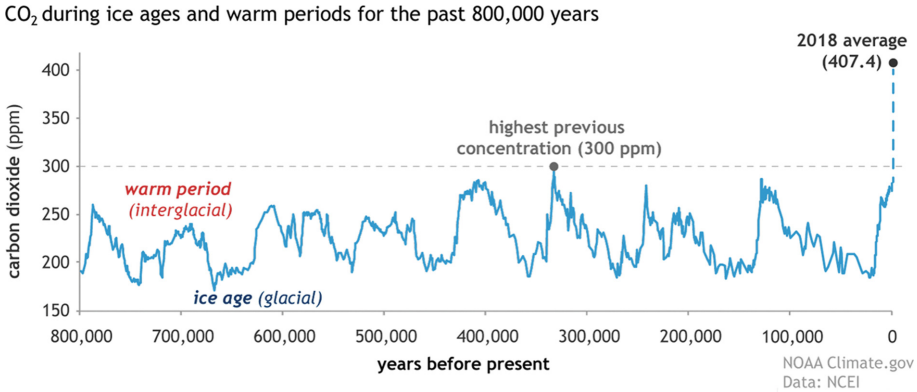

Fig. 1. Average atmospheric CO_2 concentration in the past 800,000 years. Reproduced with permission from Lindsey [1]. Copyright 2020 NOAA Climate.gov.

†To whom correspondence should be addressed.
E-mail: scudiero@wsu.edu, suha@wsu.edu

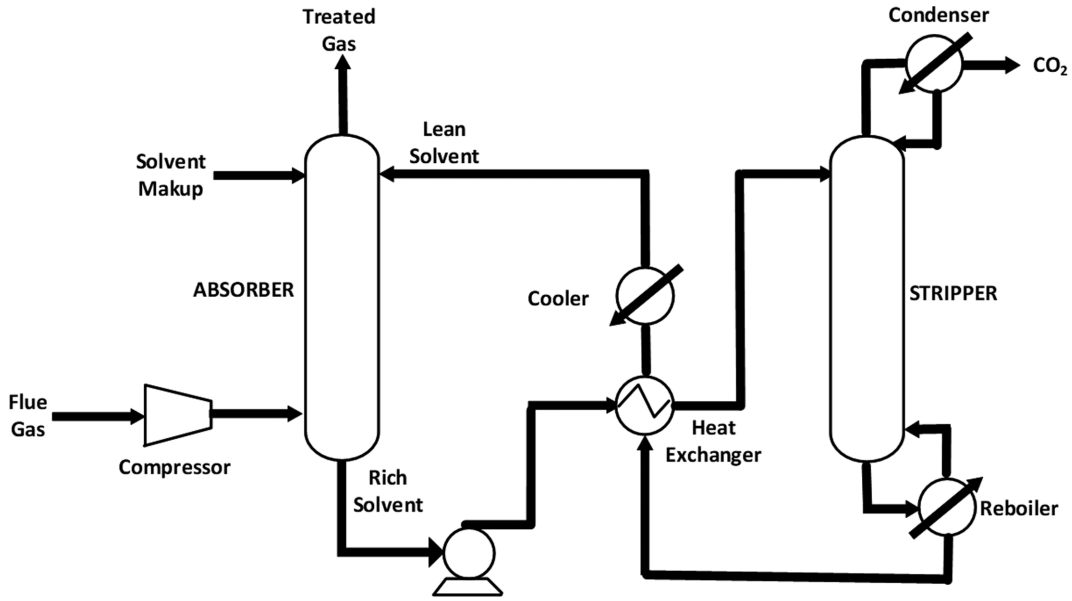

Fig. 2. Schematic of an amine-based CO_2 capture process.

be under the constant threat of high tide flooding and a projected economic cost of $1 trillion worldwide by 2050 [7,8]. To ensure the sustainability of human society, it is imperative to develop effective and sustainable energy production technologies capable of controlling and curbing the atmospheric CO_2 concentration.

2. CO_2 Capture and Sequestration Technologies

Chemical absorption using alkanolamines (RNH_2) as solvent (Fig. 2) is one of the commercially available technologies designed to capture CO_2 from large point sources, such as coal-fired power and cement production plants. The lean alkanolamine solvent is fed to the top of the absorber and the flue gas from power plants is fed to the bottom of the absorber column. Inside the absorber, CO_2 in the flue gas will react with the alkanolamine forming zwitterions ($RNH_2^+COO^-$), which will then react with RNH_2 to produce carbamate ($RNHCOO^-$) [9-13]:

$$CO_2+RNH_2 \rightarrow RNH_2^+COO^- \quad (1)$$

$$RNH_2^+COO^- + RNH_2 \rightarrow RNHCOO^- + RNH_3^+ \quad (2)$$

The CO_2-rich solvent (*the rich solvent*), which exits at the bottom of the absorber, is preheated and fed to the top of the stripper. Inside the stripper column, steam generated by the reboiler at the bottom of the stripper column provides heat to break the chemical bonding between the absorbed CO_2 and alkanolamines (e.g., monoethanolamine (MEA)). The steam then carries the desorbed CO_2 to the top of the stripper. The regenerated solvent (*the lean solvent*), which is nearly free of CO_2 is cooled and recycled back to the top of the absorber column. However, the regeneration of the alkanolamine solvent is energy-intensive. Once a CO_2 capturing process is installed in a coal fire power plant, it is reported that the energy efficiency of the power generation is reduced by about 10% and double the price of the generated electricity [9,10]. A heat exchanger can be installed to utilize the hot *lean solvent* to heat the *rich solvent* from the stripper and reduce the required energy consumption to cool the *lean solvent* before it enters into the absorber. Ongoing efforts have been made to further reduce the total energy consumption of the CO_2 capturing process by introducing an intercooling absorber, an interheating stripping device, and a cold-rich solvent split [14,15].

The captured CO_2 out of the condenser from the amine-based CO_2 capture process can be stored or utilized in the following ways:

(a) Geological sequestration: Primary and secondary oil recovery can typically produce 38% of the total amount of oil stored inside an oil field. Since supercritical CO_2 is completely miscible in oil, it can be injected into oil reservoirs to displace the residual oil and recover an additional 17% of the total amount of oil inside the reservoirs. After the oil recovery, part of the injected CO_2 can be stored inside the reservoir. The maximum capacity of geological reservoirs worldwide can store the total global CO_2 emission for at least 124 years and the total cost of CO_2 capture, transport, and storage into a geological reservoir is reported to be $16.6-91.3 USD/ton of CO_2 [16]. For geological sequestration to gain traction and public acceptance, the CO_2 potential leakage from storage sites through caprock and permeable pathways has to be addressed [17]. The annual rate of CO_2 leakage needs to be kept below 0.1%; only then can geological sequestration be an effective strategy to reduce the emission of CO_2 into the atmosphere [18].

(b) Thermochemical conversion: CO_2 can be used as an alternative carbon source to produce liquid fuel via combining the reverse water gas shift reaction and the Fischer-Tropsch reaction as shown in Fig. 3. This process begins with utilizing renewable electrical energy to produce hydrogen gas (H_2) and O_2 from the electrolysis of liquid water:

$$2H_2O \rightarrow 2H_2+O_2 \qquad \Delta H^0_{298}=242\ kJ/mol \quad (3)$$

The produced H_2 is then introduced into the reverse water gas shift reactor (RWGS) with the CO_2 gas to produce CO and H_2O (Eq. (4)), the condenser to remove H_2O, and the Fischer-Tropsch reactor (F-T) with the generated CO gas and H_2 gas from the water

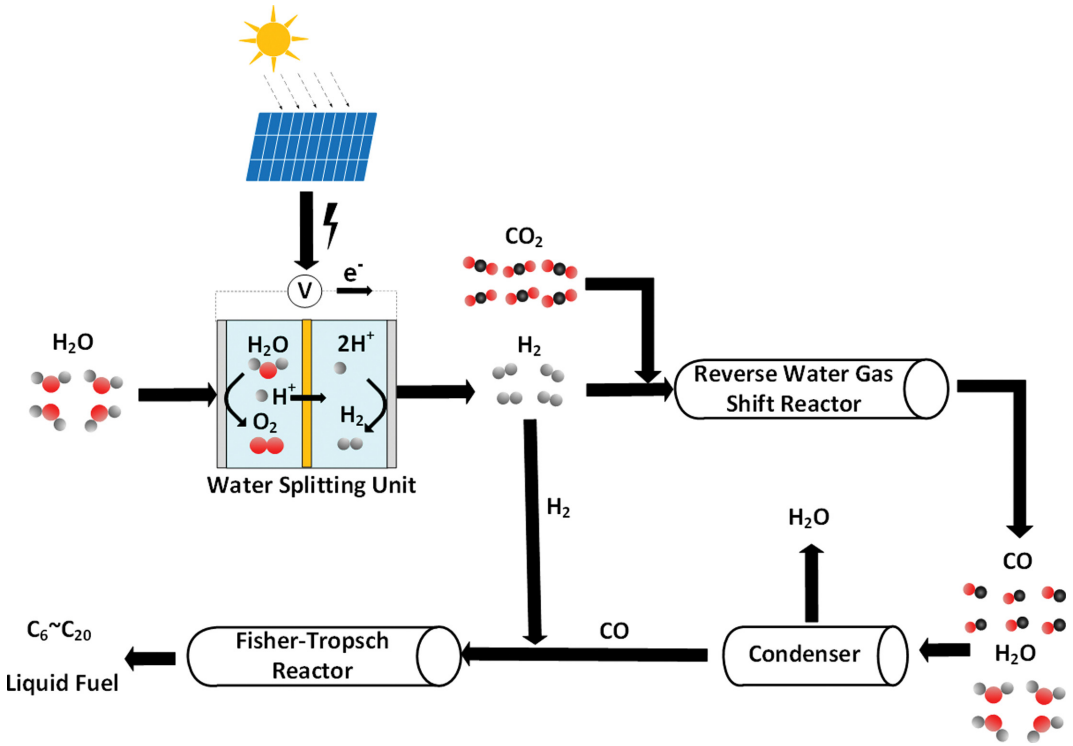

Fig. 3. Sustainable thermochemical conversion of CO_2 into liquid fuel.

electrolyzer to make liquid fuel:

$$CO_2+H_2 \leftrightarrow CO+H_2O \qquad \Delta H^0_{298}=41.2\ kJ/mol \tag{4}$$

Because the RWGS is an endothermic reaction, its reactor needs to be operated at a high temperature (>700 °C) to suppress water gas shift. At this high operating temperature, the undesired methanation reaction also could be prevented. However, even at 800 °C, the equilibrium CO_2 conversion is only 66% [19]. To further increase its CO_2 conversion, the excess amount of H_2 (e.g., the H_2/CO_2 molar ratio greater than 2) could be used, which increases its overall operation cost [19]. The H_2/CO ratio of the inlet stream to the F-T reactor needs to be adjusted for the optimum value of ~2 by feeding additional H_2 as shown in Fig. 3. In the F-T reactor, the liquid fuel is produced via the following polymerization reactions [20]:

$$nCO+(2n+1)\ H_2 \rightarrow C_nH_{2n+2}+nH_2O \tag{5}$$

$$nCO+2n\ H_2 \rightarrow C_nH_{2n}+nH_2O \tag{6}$$

$$nCO+2n\ H_2 \rightarrow C_nH_{2n+2}+(n-1)H_2O \tag{7}$$

The products coming out of the F-T reactor will consist of hydrocarbons with different chain lengths and water. The distribution of the different products is given by the Anderson-Schulz-Flory equation and plotted against the probability of chain growth (Fig. 4) [21]:

$$W_m=((1-\alpha)\alpha^{m-1}) * m \tag{8}$$

where W_m is the weight fraction of hydrocarbons with chain-length (m) and chain-growth probability (α). F-T reactors are typically operated at 220-350 °C and 10-60 bar. Since F-T reactions are exothermic, the reactor temperature must be carefully controlled. High reactor temperature closer to 350 °C will promote the undesirable formation of methane (CH_4) and carbon deposition, which will decrease the average chain length of the products and deactivate the catalyst.

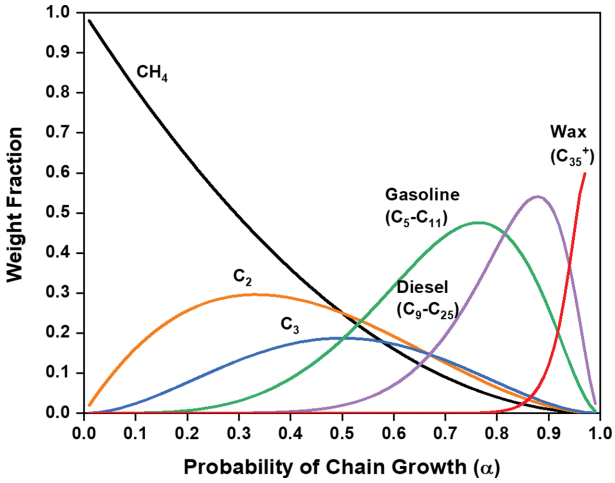

Fig. 4. Anderson-Schulz-Flory product distribution.

Although high-quality liquid fuel can be produced via the thermochemical conversion of CO_2 as described in Fig. 3, there are several technical and economic challenges:

a) *High energy consumption*: The RWGS reactor needs to be operated at high temperature and the F-T reactor needs to be operated at high pressure.

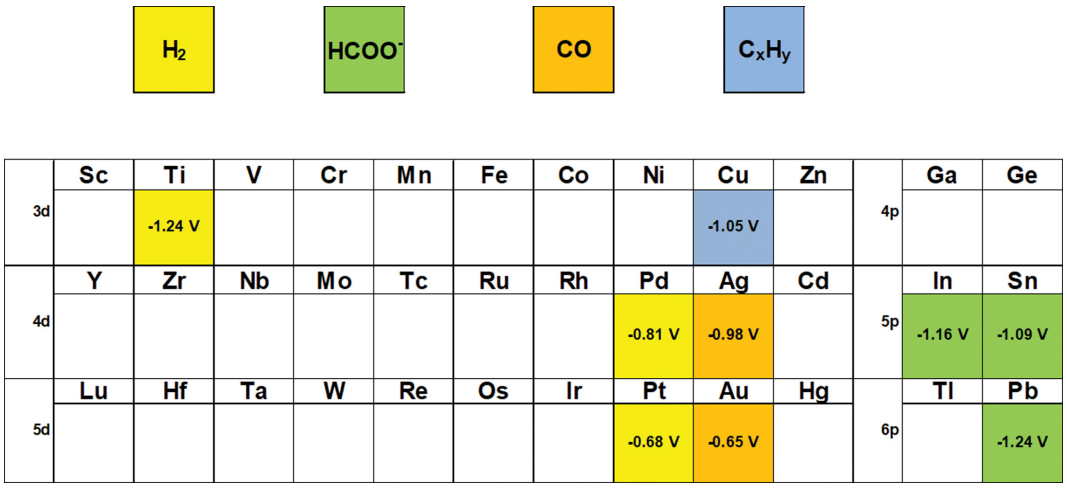

Fig. 5. The product distribution of eCO_2R reactions at $-5\ mA/cm^2$ on various transition metal electrodes in CO_2 saturated 0.1 M $KHCO_3$ (the reduction potentials are reported at SHE scale) [22].

b) *Low product flexibility*: The existing catalyst inside the F-T reactor needs to be replaced entirely with different catalysts to modify the product selectivity of the reaction.

ELECTROCHEMICAL REDUCTION OF CO_2 (eCO_2R) PROCESS

1. The eCO_2R Reaction Chemistry and Selectivity

The eCO_2R reaction is considered to be a promising technology that outperforms the thermochemical conversion of CO_2. Due to the high energy barrier of the CO_2 activation process via RWGS and CO hydrogenation via F-T, the thermochemical conversion process requires high energy input. Furthermore, an excess amount of H_2 gas from the water electrolyzer is required to hydrogenate the CO. To meet this excess amount of H_2 gas requirement, an additional capital investment and energy supply for the large-scale water electrolyzer would be needed. On the other hand, the eCO_2R process utilizes electrical energy to activate the CO_2 reaction at the cathode, which allows the use of the eCO_2R reaction at room temperature:

$$xCO_2+yH^++ne^-\rightarrow Product+zH_2O \quad (9)$$

In addition, the introduction of H_2 gas is no longer needed because the CO_2 electrolytic cell can directly utilize water to produce protons via the water oxidation reaction over the anode:

$$2H_2O\rightarrow 4H^++O_2+4e^- \quad (10)$$

An ion-conducting membrane is positioned in an electrolytic cell to separate the anode from the cathode and to prevent the mixing of the reactants and products from the anode and cathode, which would decrease the overall system efficiency. The composition of the cathode, which is usually made of transition metals, is found to have a significant influence on the product selectivity in the eCO_2R process. Hori studied the product distribution on different transition metals at the constant total current density of $5\ mA/cm^2$ in CO_2 saturated 0.1 M $KHCO_3$ [22] (The results are shown in Fig. 5). On the surface of these metals, CO_2 can be converted into CO, formate ($HCOO^-$), methane (CH_4), methanol (CH_3OH), and C_2 compounds including ethylene (C_2H_4), acetate (CH_3COO^-), and ethanol (C_2H_5OH). For instance, the primary product of the eCO_2R

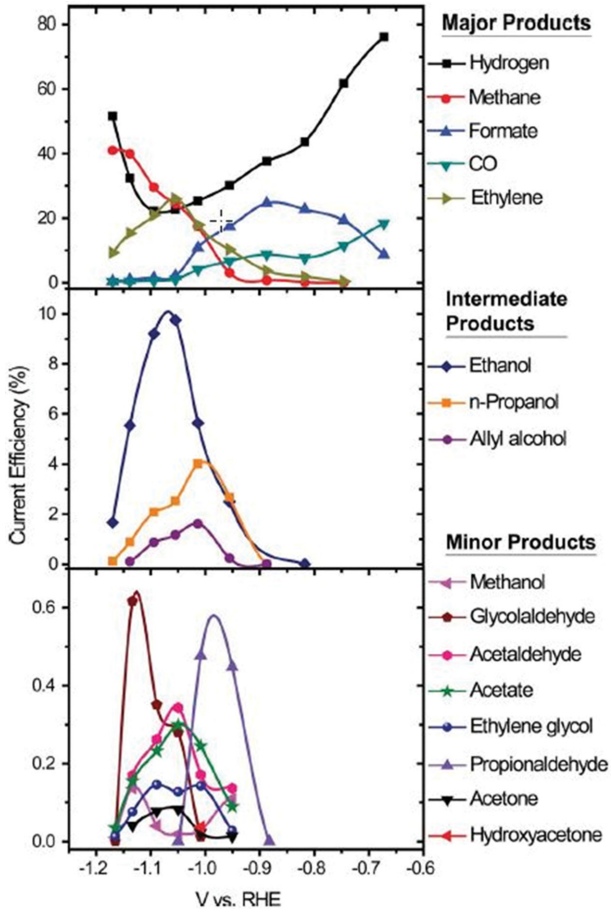

Fig. 6. Current efficiency of eCO_2R products on the surface of copper as a function of applied potential in CO_2 saturated 0.1 M $KHCO_3$ (pH=6.8). Reproduced from Kuhl et al. [23] with permission from The Royal Society of Chemistry.

reaction on indium, tin, and lead is $HCOO^-$. On platinum and titanium, the hydrogen evolution reaction (HER) is much more favorable than the eCO_2R reaction. On silver and gold, CO is the primary product of the eCO_2R reaction. Finally, copper has attracted much attention since it is the only metal promoting CO_2 conversion into C_2 hydrocarbons.

However, the selectivity of the eCO_2R process is not only influenced by the material of the cathode, but also by the reduction potential. Kuhl et al. studied the eCO_2R reaction on a copper electrode in a nearly 0.1 M $KHCO_3$ as shown in Fig. 6 [23]. The data indicate that H_2, CO, and $HCOO^-$ are the primary products at lower reduction potential. When there is enough CO on the surface, C_2H_4 and CH_4 as primary products and C_2H_5OH as intermediate products begin to be produced at a reduction potential of approximately −0.9 V vs. RHE. As the reduction potential continues to increase (i.e., <−0.9 V vs. RHE) and the amount of CO on the surface of the catalyst is sufficient, the production of C_2 compounds continuously increases consuming the surface CO. Eventually, as the negative potential reaches about −1.1 V vs. RHE, the supply of surface CO becomes insufficient, and the selectivity toward C_2 decreases. At that point, the primary products become CH_4 and H_2. Thus, the Faraday efficiency (FE%) of C_2 compound reaches its maximum at −1.05 V vs. RHE. As for palladium, Min et al. discovered that palladium could convert CO_2 into formate at very high Faradaic efficiency (>95%) in 0.5 M $KHCO_3$ when the applied potential was controlled between −0.15 V and 0 V vs. RHE [24]. However, its product selectivity toward CO would dramatically increase if the applied reduction potential was higher than −0.2 V vs. RHE (i.e., <−0.2 V vs. RHE) [25]. When its applied potential decreased lower than −0.6 V vs. RHE, the hydrogen evolution reaction became the dominant reaction and the primary product was hydrogen gas [26]. These results indicate that the product selectivity can be controlled by tuning the reduction potential without replacing the catalyst. Therefore, combining the eCO_2R process with renewable energy, the eCO_2R reaction is a promising solution to close the carbon cycle while providing opportunities to produce value-added chemicals and fuel derivatives. In the following section, the techno-economic analysis of the eCO_2R process is first briefly discussed. Next, the two most commonly used cell configurations, H-cell and gas diffusion electrode (GDE), are explained.

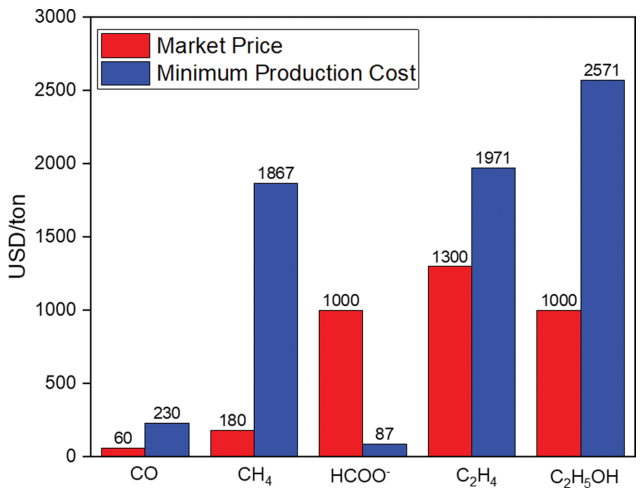

Fig. 7. Market price and minimum production cost of primary eCO_2R products (metric ton/day).

Table 1. Parameters used to conduct the economic analysis [24,29-32]

Product	No. e^-	Cell voltage (V)	Faradaic efficiency
CO	2	1.5	96%
CH_4	8	2.38	76%
$HCOO^-$	2	1.86	95%
C_2H_4	12	2.67	70%
C_2H_5OH	12	2.68	29%

2. Techno-Economic Analysis and Selection of Desired Products

Fig. 7 shows the market price and minimum production cost of primary products from the eCO_2R process [27]. The minimum production cost consists of the CO_2 capture and storage costs at a coal-fired power plant and the electricity cost for electrochemically converting the captured CO_2 into value-added chemical products. For the minimum cost estimation, we assume that the CO_2 capture cost from the flue gas stream using the MEA-based chemical absorption technology is \$70/ton of CO_2 and the solar electrical power cost is \$40/MWh [28,29]. The electricity cost needed to produce one metric ton of product per day is estimated by:

$$\text{Cell Voltage} * 1{,}000 \frac{\text{kg}}{\text{day}} * \frac{1}{86{,}400} \frac{\text{day}}{\text{second}} * \frac{1}{\text{MW}} * \frac{1}{\text{Faradaic efficiency}} * n * 96{,}485 * \$40/\text{MWh} \quad (11)$$

where MW is the molecular weight of the product, n represents the number of electrons needed to convert one CO_2 molecule into one molecule of desired product. All the parameters used for the calculation are summarized in Table 1 [24,30-33]:

The techno-economic analysis indicates that the production of formate ($HCOO^-$) from the eCO_2R process is very profitable and competitive compared to its market value. $HCOO^-$ is widely used as a drilling fluid in the oil and gas industry, a deicing agent, fertilizer, and heat transfer fluid. Moreover, $HCOO^-$ can be used as an energy carrier in a direct formate fuel cell (DFFC) to generate electricity. The latter provides an opportunity to develop a sustainable regenerative energy system by combining an eCO_2R unit and a DFFC as shown in Fig. 8, which can store renewable energy in the form of $HCOO^-$ during the "charging phase" and provide electricity during the "discharging phase" without the net CO_2 emission. Moreover, the eCO_2R into $HCOO^-$ is a single-step reaction that is highly energy-efficient. On the other hand, the cost of producing CO, CH_4, and C_2H_5OH from the eCO_2R process is much higher than their market values. For instance, ethanol (C_2H_5OH) is already being mass-produced using starch-based crops such as corn and wheat. Thus, it may not be cost-effective to produce C_2H_5OH via the eCO_2R process.

Even though the ethylene (C_2H_4) market price is lower than that of the minimum cost of the eCO_2R process, the difference is much smaller compared to the CH_4 and C_2H_5OH cases. The market competitiveness of ethylene production via the eCO_2R process is promising because C_2H_4 is currently produced in the industry via the

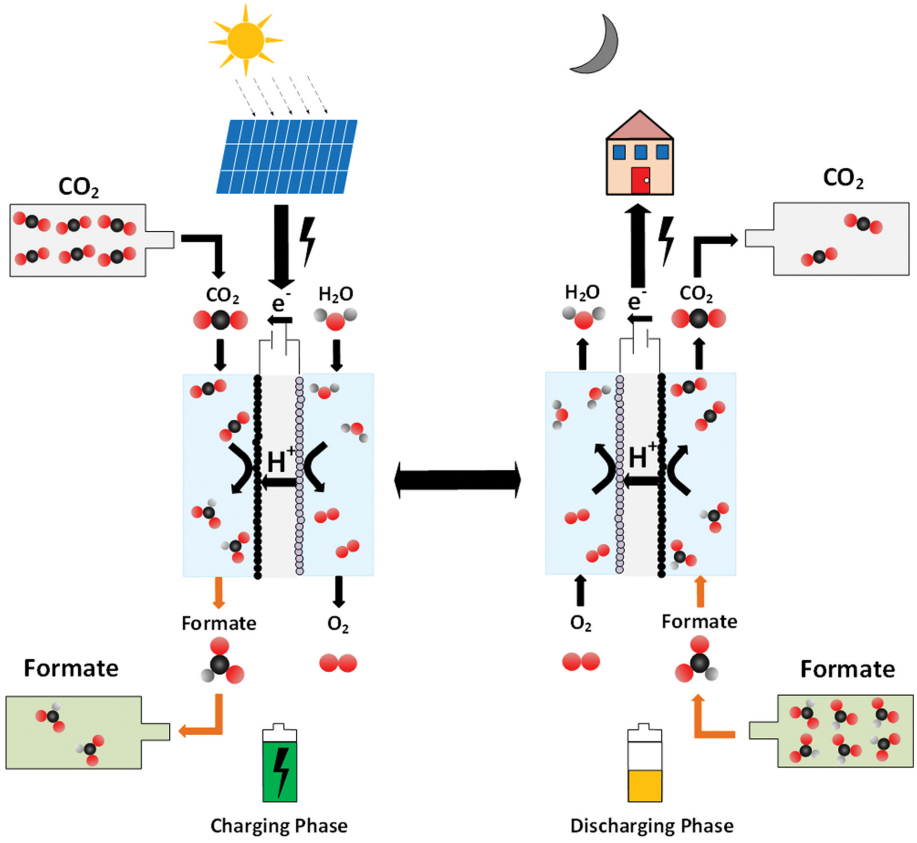

Fig. 8. Schematic of a regenerative energy system using $HCOO^-$ as an energy carrier.

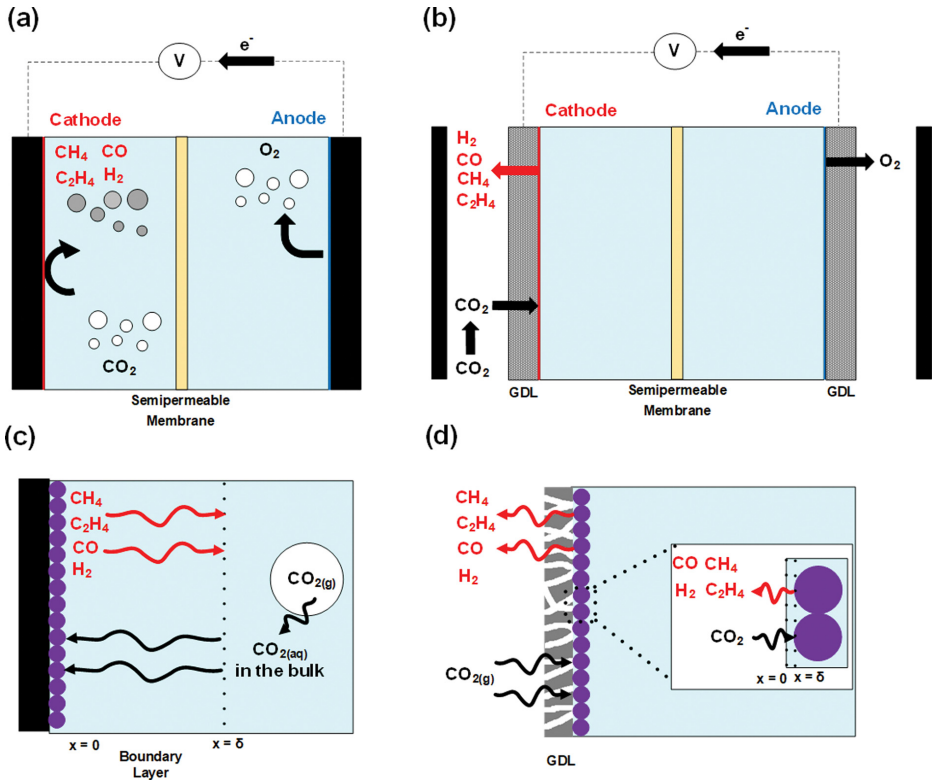

Fig. 9. Schematic of (a) an aqueous fed and (b) a gaseous fed CO_2 electrolyzer (GDE), (c) CO_2 barrier diffusion layer (d) at the cathode inside an aqueous fed electrolyzer, and (d) reduced CO_2 barrier diffusion layer (δ) at the cathode inside a gaseous fed electrolyzer.

energy-intensive steam cracking process at 750-950 °C, which requires the consumption of 13.8 GJ/ton and generates 39 Mton of CO_2 [34]. An alternative to steam cracking could be the eCO_2R process if the electricity price from the solar farms could be decreased below $24.6/MWh. Since the eCO_2R process consumes CO_2, it could be a more economically attractive process than the conventional steam cracking process if the carbon tax is added to the economic analysis. Therefore, for the rest of this review paper, we discuss the current progress in the eCO_2R technology for the production of both $HCOO^-$ and C_2H_4.

3. Configuration of CO_2 Electrolyzers (Aqueous CO_2 Input vs. Gaseous CO_2 Input)

Two main factors that influence the performance of a CO_2 electrolyzer are (1) the mass transfer of CO_2 from the atmosphere to the electrode surface via the liquid electrolyte and (2) the kinetic energy barrier of reducing CO_2 at the electrode surface. The local CO_2 and proton concentrations at the surface of the cathode will decrease as the rate of CO_2 reduction increases. If the CO_2 concentration at the cathode surface decreases too low at a sufficiently high CO_2 reduction rate, the overall reaction rate of the eCO_2R process will be limited by the poor CO_2 mass transfer. The CO_2 electrolyzer can be classified as an aqueous fed and gaseous fed electrolyzer. Inside an aqueous fed CO_2 electrolyzer, CO_2 is introduced into the cell by bubbling CO_2 gas directly into the electrolyte (Fig. 9(a)). The CO_2 dissolves at the gas-liquid interface of the bubbles, forming aqueous CO_2, and then diffuses to the surface of the cathode (Fig. 9(c)). However, the maximum CO_2 reduction current density (j_{max}<50 mA/cm^2) that can be achieved inside this type of electrolyzer is insufficient for practical utilization. The low current density is due to the 40-200 μm thick boundary layer (δ) that the dissolved CO_2 has to diffuse to reach the surface of the cathode, as shown in Fig. 9(c) [35,36].

To reduce the diffusion barrier and boost j for the practical application of the CO_2 reduction technology, a new design of the gas diffusion electrode (GDE) was proposed (Fig. 9(b)). An electrocatalyst layer is deposited on the cathode surface forming a gas diffusion layer (GDL). The GDL is usually a porous carbon paper coated with hydrophobic polytetrafluoroethylene (PTFE) to achieve the desired water management and prevent flooding inside the paper. Since the catalyst layer is usually hydrophilic, a very thin layer of electrolyte will form on the surface of the catalyst. Then, CO_2 gas, which flows through the GDL, dissolves into this thin liquid electrolyte layer and only needs to diffuse through 0.01 and 10 μm thick of the electrolyte layer (i.e., a much-reduced boundary layer) to reach the surface of the catalyst as shown in Fig. 9(d) [37]. With the enhanced supply of CO_2 to the catalyst surface, the j produced by this GDE configuration can typically exceed 100 mA/cm^2 [33, 37-39].

ELECTROCHEMICAL REDUCTION OF CO_2 INTO $HCOO^-$

The choice of the electrocatalyst layer on the cathode has a significant influence on the selectivity and energy efficiency of a CO_2 electrolyzer. Based on the techno-economic analysis, the eCO_2R technology for producing $HCOO^-$ has a great potential of commercialization if the following performance benchmarks can be achieved: (1) reduction current density (j)>300 mA/cm^2, (2) overpotential< 0.5 V, and (3) Faradaic efficiency (FE_{HCOO^-})>70% [27]. The use of transition metals as the electrocatalyst for eCO_2R has been studied for decades. These studies indicate that CO_2 can be converted into $HCOO^-$ over metal surfaces such as In, Sn, Pb, Bi, and Pd [22,24,40]. According to their corresponding minimum overpotential required to convert the CO_2 into $HCOO^-$ via the eCO_2R process, these five metals can be classified into two categories:

(1) overpotential>1 V: In, Sn, Pb, and Bi

(2) overpotential<0.2 V: Pd

For the commercial utilization of In, Sn, Pb, and Bi-based electrocatalysts, their required minimum overpotential needs to be reduced. For Pd-based electrocatalyst, its material cost needs to be reduced by maximizing its material utilization.

1. Monometallic Electrocatalysts

1-1. Electrocatalysts Requiring High Overpotential for eCO_2R into $HCOO^-$

In, Sn, Pb, and Bi monocatalysts require applied potential between −1.6~−2.2 V vs. Ag/AgCl to facilitate the CO_2 reduction into HCOOH and to achieve a FE_{HCOO^-} of least 70% [41-46].

Feaster et al. discovered a volcano plot of the HCOOH reduction current vs. BE_{*OCHO} via density functional theory calculation as shown in Fig. 10, which indicates *OCHO may be the key intermediate species of CO_2 reduction into HCOOH [47]. This result suggests that the surface binding strength of *OCHO (BE_{*OCHO}) has a significant impact on the activity of the catalyst toward the production of HCOOH. If the binding energy is too high, *OCHO will act as the poisoning species blocking the surface-active sites. If the binding energy is too weak, the formation of *OCHO will be prohibited and act as the rate-limiting step for the overall eCO_2R process to produce HCOOH. This plot indicates that Sn has the highest catalytic activity toward the eCO_2R into HCOOH because it offers the optimum BE_{O*CHO} (i.e., not too strong and not too weak). However, the plot does not include In, Pb, and Bi, which have also been identified to produce HCOOH efficiently.

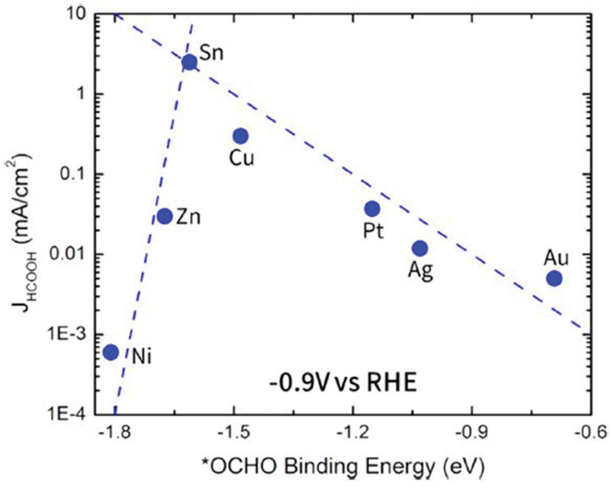

Fig. 10. Volcano plot of HCOOH partial current vs. BE_{*OCHO}. Reprinted with permission from Feaster et al. [47] Copyright 2017 American Chemical Society.

To increase the total current for the eCO_2R process, prepared nanomaterials require higher electrochemical active surface areas. Furthermore, having lower coordinated active sites on the surface has been proven to reduce the kinetic barrier of forming the intermediate species, *OCHO, and increase the activity toward the eCO_2R to form $HCOO^-$ [48,49]. Lower coordinated active sites are usually more exposed on the surface of nanomaterial with smaller sizes [50,51]. Ávila-Bolívar et al. prepared carbon-supported Bi nanoparticles with 10 nm of particle size [52]. The FE_{HCOO^-} and j reached 100% and 15 mA/cm^2 at −1.5 V vs. Ag/AgCl, respectively. Luo et al. prepared a three-dimensional porous In-based electrode that could convert CO_2 into $HCOO^-$ with a FE_{HCOO^-} of 90% at −1.6 V vs. Ag/AgCl [53]. The value of j was measured to be 12.5 times higher than for In foil at the same applied potential. In addition to the size effect, the number of lower coordinated sites could be changed by controlling the morphology of the surface and creating additional edges and corners for the nanoparticles. Qiu et al. prepared oxide-derived Bi nano-flower with a vast number of edge sites via the reduction of Bi_2O_3 nanorods. The catalyst converted CO_2 to $HCOO^-$ with a FE_{HCOO^-} of 99.2% over 20 hours span [54].

Aiming to reduce the mass transfer resistance and increase the value of j for the production of $HCOO^-$, Sn catalyst was used in several studies. Castillo et al. investigated the particle size effect of Sn nanocatalysts on the performance of GDE for the production of $HCOO^-$ from the eCO_2R process [55-57]. The GDE with 10-15 nm Sn nanoparticles at the cathode converted CO_2 into $HCOO^-$ with a FE_{HCOO^-} of 70% and a current density (j) of 150 mA/cm^2 at the cathode potential of −1.5 V vs. Ag/AgCl. The average $HCOO^-$ production rate of the GDE was reported to reach 5.45 $mmol/m^2$-sec. Lee et al. designed a GDE without liquid electrolyte for the cathode to produce $HCOO^-$ using commercial Sn nanoparticles [58]. Humidified CO_2 was fed into the cathode side of the GDE and the amount of water vapor in the CO_2 gas flow was controlled by the temperature of a bubble humidifier. 1 M KOH was used as the anolyte. The catholyte-free GDE could produce $HCOO^-$ with a stable FE_{HCOO^-} of 91.2% at the cell potential of 2.2 V for 48 hours, while FE_{HCOO^-} of the GDE using KCl as the catholyte dropped more than 50% after 48 hours of operation.

1-2. Electrocatalyst Requiring Low Overpotential for eCO_2R into $HCOO^-$

Pd is one of the most efficient electrocatalysts with the capacity of converting CO_2 into formate at low overpotential ($0<\eta<0.2$ V) with very high FE_{HCOO^-} (>95%) [24]. Fig. 10 shows a possible reaction mechanism of eCO_2R into $HCOO^-$ on the surface of Pd [24, 59].

At nearly 0 V vs. RHE, Pd forms palladium hydride (Pd-H) [60]. The nucleophilic surface hydride will attack the electrophilic carbon atom in a CO_2 molecule, initiating a proton-electron transfer, which leads to the production of *HCOO intermediate species. Podlovchenko et al. and Min et al. discovered that this initial electron transfer is the rate-limiting step [24,59]. After the intermediate species *HCOO is formed, it rapidly reduces into $HCOO^-$ after it receives one more electron from the cathode of the electrolytic cell. When the applied reduction potential is higher than −0.2 V vs. RHE at pH=7, the reaction selectivity toward the CO starts to increase at the cost of the $HCOO^-$ selectivity [61]. Since the Pd surface can be quickly poisoned by CO, the optimal range of applied potential in a neutral electrolyte to produce $HCOO^-$ is reported to be between −0.2 V and 0 V vs. RHE. Under this potential range, the Pd surface could provide a high FE value (i.e., close to 99%) for formate production. However, the total current density over the Pd surface at this potential range is very small (i.e., less than 100 mA/cm^2), which limits its usage for large-scale industrial applications [24].

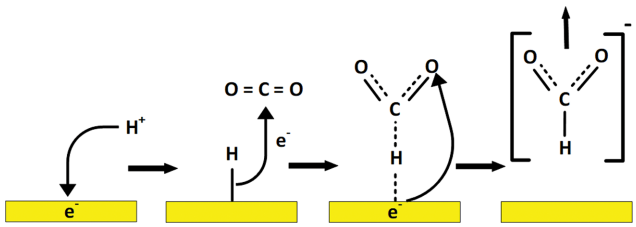

Fig. 11. Possible reaction mechanism of eCO_2R into $HCOO^-$ for Pd-based catalysts [24,59].

2. Bimetallic Pd-based Electrocatalysts

According to the possible reaction mechanisms for the conversion of CO_2 into $HCOO^-$ over Pd-based surface shown in Fig. 11, the catalytic activity can be optimized by decreasing the strength of Pd-H bonds to facilitate the bond-breaking step (i.e., the rate-limiting step of eCO_2R into $HCOO^-$). However, if the bonding strength is too weak, the intermediate species (i.e., Pd-H) will not form on the surface. Therefore, the concentration of Pd-H will be too small to facilitate the eCO_2R process to produce $HCOO^-$. To maximize the activity of the electrocatalyst, the strength of Pd-H needs to be optimized. This objective can be achieved via changing the electronic properties of the metals. Hammer et al. proposed d-band theory to describe the correlation between the electronic properties of transition metals and their surface chemical properties [62]. Once molecules are adsorbed on the transition metal surface, the metal d-band orbital couples with the bonding orbital (σ) of the adsorbate and splits into bonding state (d-σ) and antibonding state (d-σ)* as shown in Fig. 12. The electronic structure of the metal dictates the extent of the electron filling of the (d-σ)* state. As the electrons fill the (d-σ)* state, the bonding strength between the

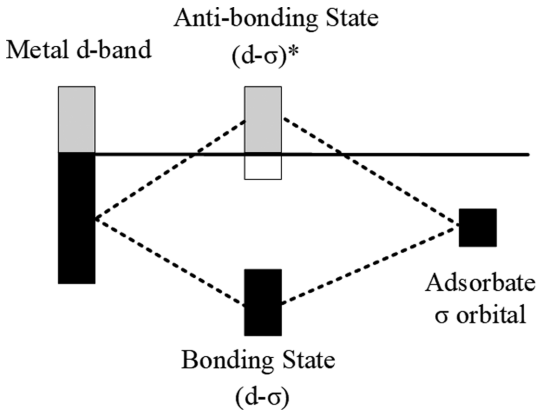

Fig. 12. Schematic of the d-band theory [62].

surface and the adsorbate is weakened. Since the position of the d-band center is highly correlated with the extent of the electron filling to the (d-σ)* state, it can be used as an indicator of the surface bonding strength. If the d-band center moves away from the Fermi level, the antibonding states are emptied resulting in a strengthening of the chemical bond between metal and adsorbate, and vice-versa.

Furthermore, the position of the d-band center between different transition metals can be altered by two types of interaction: the ligand effect and the strain effect. Using two transition metals with a different fraction of empty states to form an alloy or a layered bimetallic material will initiate charge transfer from the metal with the lowest fraction of empty states to the one with the highest fraction of empty states (ligand effect). Therefore, the shift of the d-band center away from the Fermi level of the metal with the highest fraction of empty states increases the electron filling of the antibonding states, which eventually weakens the bond strength between the adsorbate and the metal surface.

The structural strain also changes the position of the d-band center [62]. When there is a compressive strain on the surface, the overlap of the metals d states at neighboring sites and the size of the d-band width will increase. To maintain a constant filling, the d-band center moves away from the E_F (as shown in Fig. 13) and the bonding between the surface and the adsorbate weakens. The lattice strain can be originated by (1) atomic size mismatch: adding atoms with larger size into a crystal structure will expand the structure and cause tensile strain, and (2) lattice mismatch: structure strain exists at the interface of two heterogeneous metal layers. Once a bimetallic alloy or layer material is prepared, the ligand effect and the strain effect at the bimetallic interface can be used to modify the surface chemical properties.

Although CO_2 can be converted into formate at very low overpotential on the surface of pure Pd, the major challenges using Pd as the electrocatalyst for CO_2 reduction are its low long-term stability caused by CO poisoning and high material cost. Preparation of Pd-based bimetallic alloys and overlayer using another metal is proven to be able to reduce CO poisoning.

If the Pd-based bimetallic catalyst utilizes inexpensive non-noble metals, the bimetallic approach will also reduce the cost of the catalyst synthesis. Kortlever et al. prepared carbon-supported Pd-Pt alloy particles (Pd-Pt/C) with different Pd contents [63]. At −0.42 V vs. RHE, the maximum concentration of formic acid per mg of $Pd_{70}Pt_{30}$/C produced on the surface of the catalyst in CO_2 saturated 0.1 M K_2HPO_4/KH_2PO_4 (pH=6.7) was 12.7 times higher than

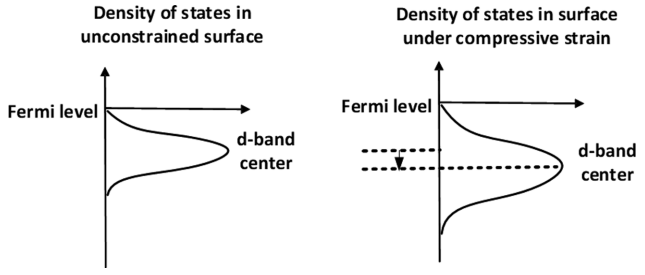

Fig. 13. Strain effect on the d-band center [62].

the concentration produced on the surface of Pd/C. Another study by Jiang et al. indicates that the activity and stability of Pd could be improved by doping boron into Pd (Pd-B/C) [64]. Their density functional theory calculations showed that doping Pd with boron makes the kinetic pathway of eCO_2R into $HCOO^-$ more favorable than that of eCO_2R into CO, which increases the catalytic activity toward the $HCOO^-$ production and makes the surface less susceptible to CO poisoning. Their XPS measurements show an uplift of the d-band center away from the Fermi-level after boron doping, which indicates that the selectivity of the catalyst toward the $HCOO^-$ formation increased by decreasing the bonding strength between the surface and the intermediate species (e.g., Pd-H). At −0.5 V vs. RHE, the maximum concentration of formic acid per mg of Pd produced on the surface of Pd-B/C in CO_2 saturated 0.1 M $KHCO_3$ was 18 times higher than the concentration produced on the surface of their homemade Pd/C. A study by Wang et al. on carbon-supported CuPd nanoparticles (CuPd/C) with different Cu bulk molar concentration prepared via the adsorbate induced surface segregation method indicates that adding Cu into the lattice structure of Pd forming a bimetallic CuPd alloy lowered the d-band center of Pd away from the Fermi-level and weakened the bond strength of Pd-H, increasing the total reduction current density and the FE_{HCOO^-} [65]. However, they also found that having too much Cu (larger than 60 mol%) significantly decreased the activity of the catalyst toward CO_2 reduction into $HCOO^-$.

ELECTROCHEMICAL REDUCTION OF CO_2 INTO C_2 COMPOUNDS

1. Cu-based Electrocatalyst

Carbon monoxide (CO) has been identified as the key intermediate species of the eCO_2R into C_2 compounds [66,67]. The binding energy of CO on the metal surface has a significant impact on the product selectivity of the eCO_2R reaction. If the CO binding energy is too low, CO molecules desorb from the surface before it can be further converted into C_2 compounds. If the CO binding energy is too high, CO molecules stick to the surface blocking active sites and act as the poisoning species. Among the transition metals, Cu is reported to possess a suitable CO binding energy that can allow the conversion of CO_2 into C_2 compounds [39,68-70].

Fig. 14 describes the possible reaction mechanisms of eCOR into C_1 and C_2 compounds on the surface of Cu [71,72]. If the CO coverage of the surface is low, then the CH_4 formation reaction will be more favorable over the C-C coupling reaction. According to Fig. 14, there are two possible pathways to produce CH_4 over the Cu surface from CO_2: the CHO and COH pathways. Absorbed CO molecules undergo a proton-electron transfer (P-E T) forming *CHO or *COH. Both species undergo two additional P-E T to form *CH and H_2O. The *CH species goes through three additional P-E T to form CH_4 and H_2O as the by-product.

If the CO coverage of the surface is high enough, the C-C coupling reaction may occur between two CO molecules to form *CO-*CO (the CO-CO pathway) as shown in Fig. 14. The *CO-*CO will then undergo a P-E T to form *CO-*COH. In addition, the *CO-*COH species may also form via the coupling reaction between *CO and *COH (the CO-COH pathway). The *CO-

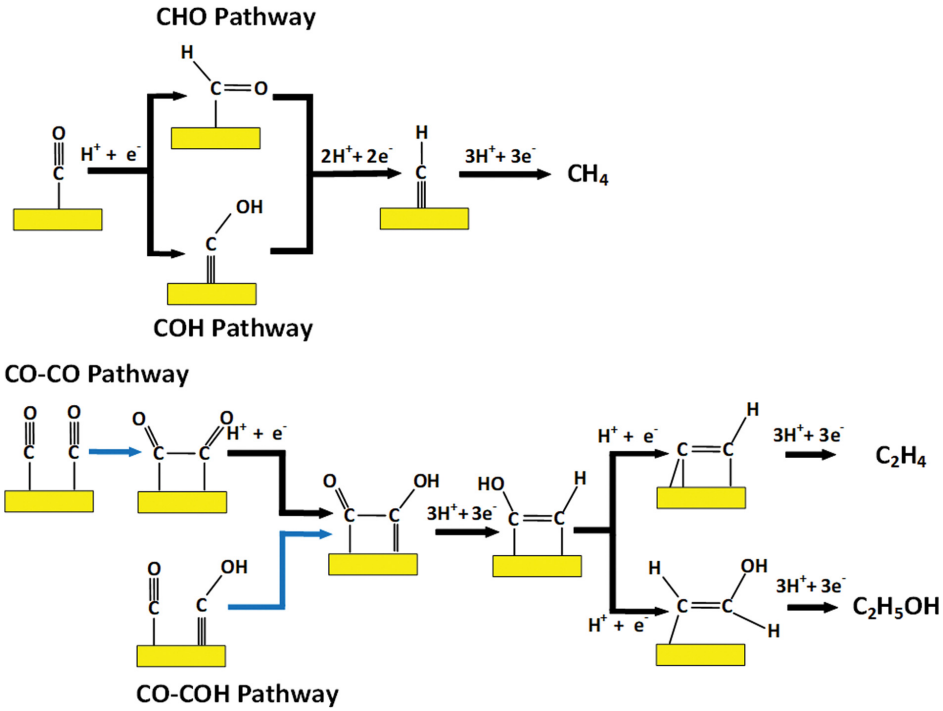

Fig. 14. Possible reaction mechanisms of eCOR into C_1 and C_2 compounds on the surface of Cu [71,72].

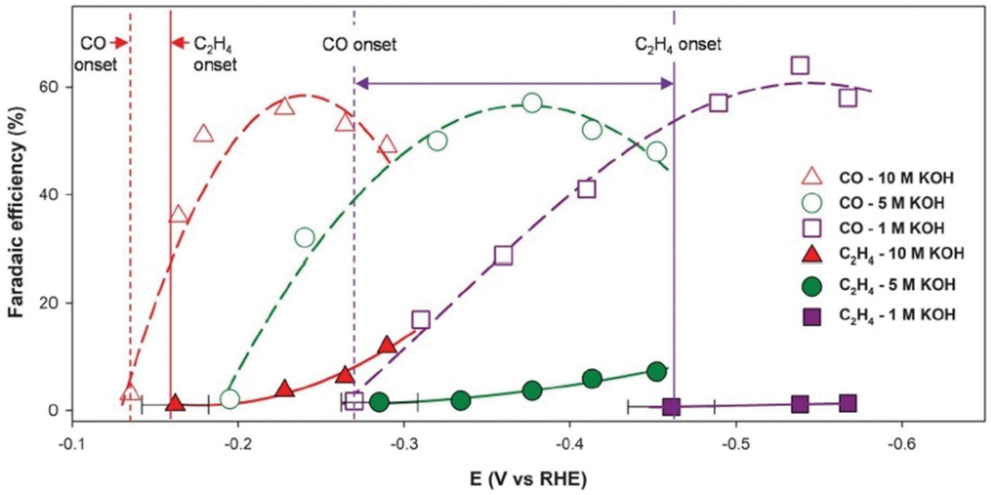

Fig. 15. FE of CO and C_2H_4 as a function of applied potential in KOH with different concentrations. From Dinh et al. [33] Reprinted with permission from AAAS.

*COH goes through three additional P-E T to form *COH=*CH and H_2O. After the *COH-*CH species undergoes one additional P-E T, two possible intermediates can be produced: *C=*CH and *CH-*CHOH. Finally, *C=*CH and *CH-*CHOH undergo an additional three P-E T to form C_2H_4 and C_2H_5OH, respectively, with H_2O as the by-product. These reactions are shown in detail in Fig. 14.

Several studies have investigated the influence of pH on the eCO_2R to produce C_2 compounds. Raciti et al. developed a transportation model to study the effect of local pH for CO_2 reduction [73]. They found that the partial current density for producing C_2 compounds increases with increasing local pH. Dinh et al. conducted the eCO_2R reaction using KOH with a concentration ranging from 1 M to 10 M to study the pH effect on the reaction. Strikingly, the onset potential for the CO_2 reduction reaction became less negative (i.e., required less overpotential) when the KOH concentration was increased, as shown in Fig. 15 [33]. In 10 M KOH, the required overpotential to drive the C_2H_4 production was only 0.245 V. Xiao et al. performed DFT calculations to investigate the dependence of the onset potential on pH for the formation of C_2 compounds [74]. The data indicate that the C-C coupling reaction is suppressed and no C_2 compounds are produced at pH=1. When the pH was increased to about 7, C_2 was produced on the

surface via both the CO-CO and the CO-COH pathways. The intermediate species, COH, was consumed to produce both C_1 and C_2 compounds. The calculated production ratio of C_2 to C_1 was 0.2 : 1. At pH=12, the production of C_2 via the CO-CO pathway was dominant over the production of C_1 via the CHO and COH pathways. The calculated production ratio of C_2 to C_1 was then 1 : 0.00001. Both the DFT calculations and the experimental data indicate that a high pH environment effectively promotes the eCO_2R into C_2 compounds.

The use of an alkaline electrolyte decreases the overpotential and increases the selectivity toward the production of C_2 compounds [75]. However, the introduction of CO_2 inside an alkaline electrolyte generates carbonate, which drastically decreases the long-term stability of the CO_2 electrolyzer:

$$CO_{2(aq)}+OH^-_{(aq)}\leftrightarrow HCO^-_{3(aq)} \quad (12)$$

$$HCO^-_{3(aq)}+OH_{(aq)}\leftrightarrow CO^{2-}_{3(aq)}+H_2O_{(l)} \quad (13)$$

The formation of carbonate not only depletes solvated CO_2 near the surface of the electrode, but also produces water molecules. Without an adequate amount of solvated CO_2, the hydrogen evolution reaction (HER) becomes the dominant reaction, and the product selectivity shifts to H_2 production instead. Moreover, water produced via the carbonation reaction could accumulate inside the GDL channels. Once the liquid penetrates the GDL and reaches the gas channel, water evaporates and crystals of K_2CO_3 can precipitate on the surface of the GDL, blocking further the CO_2 molecules from diffusing to the catalyst layer [76,77].

Since CO is the key intermediate species of the CO_2 conversion, C_2 compounds can also be produced via the two-step conversion [68,79,80]. In the first electrolyzer, CO_2 is first converted into CO using a nearly neutral electrolyte. CO is then fed into the second electrolyzer using an alkaline electrolyte to produce C_2 compounds. Since CO is very stable inside alkaline electrolytes, the formation of carbonate can be prevented. Therefore, converting CO_2 into C_2 compounds via the two-step conversion can lead to a high rate and high selectivity while improving the long-term stability. The following sections discuss the current technological advancement of CO_2 reduction into CO using a nearly neutral electrolyte and CO reduction into C_2 compounds using alkaline electrolytes.

2. The Two-step Conversion: The Reduction of CO_2 into CO

The production of CO from eCO_2R at the industrial scale has been demonstrated by Lutz et al. They designed a flow cell with a proprietary membrane, an Ag cathode, and an IrO_2 anode [80]. When their cell was operated at 2.8 V, CO was produced with 93.8% selectivity and a current density, j=300 mA/cm^2. Kutz et al. developed a membrane electrode assembly with polystyrene tetramethyl methylimidazolium chloride (PSTMIM) anion conductive membrane, Ag cathode, and IrO_2 anode [81]. At a cell voltage of 3 V, the MEA could produce CO with more than 90% selectivity and a current density of 200 mA/cm^2 for 1,000 hours. Zheng et al. developed a 10×10 cm^2 modular cell using a carbon-supported nickel single-atom catalyst that can produce CO at more than 100 mA/cm^2 with almost 100% selectivity [82]. Yin et al. developed a GDE using carbon-supported Au as the cathode and quaternary ammonia poly N-methyl-piperidine-co-p-terphenyl as the membrane electrolyte. Pure water was fed into the anode to conduct the water oxidation reaction. They reported that their cell could produce CO with a current density of 500 mA/cm^2 and an FE of 85% at a cell voltage of 3 V [83].

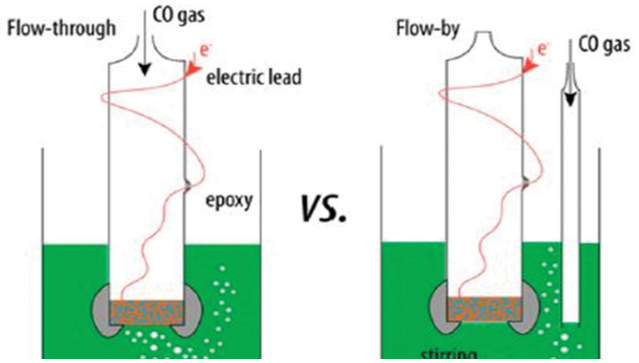

Fig. 16. Schematic of two GDEs with the flow-through and the flow-by configuration designed by Han et al. Reprinted with permission from Han et al. [84] Copyright 2018 American Chemical Society.

3. The Two-step Conversion: The Reduction of CO into C_2 Compounds Using Alkaline Electrolytes

Han et al. designed two GDEs with two different ways of introducing CO into the cells: a flow-through configuration (GDE-FT) and a flow-by configuration (GDE-FB) (Fig. 16) [84]. The CO gas flows through the electrode for the GDE-FT configuration, while the CO is bubbled into the electrolyte near the electrode for the GDE-FB configuration. The GDE-FT configuration provides a shorter CO diffusion length to the catalyst than the GDE-FB configuration. The experimental data shows that the GDE-FT configuration could convert CO into C_2H_4 in 10 M KOH with an FE= 17.8% and j=50.8 mA/cm^2. On the other hand, the GDE-FB configuration could convert CO with an FE of only 0.94% and j of 0.9 mA/cm^2. Jouny et al. designed their GDEs using oxide-derived Cu nanoparticles with a pore size of 10-20 nm as cathode, IrO_2 nanoparticles as the anode, and KOH with different concentrations as the electrolyte [85]. When their cell was operated at −0.72 V vs. RHE, the total partial current density for the formation of C_2 compounds ($j_{R,C2}$) reached 830 mA/cm^2. Gas chromatography (GC) data indicate that the FE of forming C_2H_4 and C_2H_5OH from CO was about 20% and 44%, respectively. Furthermore, the performance of CO conversion into C_2 compounds could be further enhanced using more concentrated KOH, confirming that a high pH environment indeed promoted the C-C coupling reaction. They attempted to operate the cell at a higher cell potential to increase the $j_{R,C2}$ beyond 1 A/cm^2. However, the cell performance dropped significantly after 30 mins of operation due to water accumulation inside the GDL and the gas chamber. Luc et al. studied the effect of crystal facet on the eCOR into C_2 compounds [86]. A two-dimensional Cu nanosheet was loaded on the cathode inside of their GDE. The experimental data showed that the predominant (111) surface promoted the formation of CH_3COO^- and suppressed the formation of other C_2 compounds, such as C_2H_4 and C_2H_5OH. The CO molecules could be converted into CH_3COO^- with FE of 48% and a partial current density of 131 mA/cm^2 using a 2 M KOH

electrolyte.

CONCLUSION AND FUTURE OUTLOOK

The electrochemical reduction of CO_2 (eCO_2R) reaction is a promising strategy to recycle CO_2 and produce a variety of chemicals. Compared with other CO_2 capture and conversion technologies, a CO_2 electrolyzer can be operated at low temperature and the product selectivity can be controlled by tuning the cathode applied potential. Among the chemicals, which could be produced by CO_2 reduction, the techno-economic analysis indicates that the production of $HCOO^-$ is currently economically feasible. With a further decrease in the cost of electricity produced from solar energy below $24.6 per MWh, ethylene production via the eCO_2R reaction could also become economically competitive against the conventional thermo-cracking process of ethylene production. This review discusses the current advancements of using the CO_2 electrochemical reduction reaction to produce C_1 and C_2 compounds. However, several challenges still need to be overcome and they are listed below.

1. *eCO_2R into $HCOO^-$*: Many studies have demonstrated that CO_2 could be converted into $HCOO^-$ over In, Sn, Pb, and Bi with high FE and stability. However, high overpotential (>1 V) is required to drive the reaction. Although many attempts have been made to improve the activity of electrocatalysts via tuning the particle size, synthesizing bimetallic catalysts, and increasing the number of undercoordinated active sites, most of them were unsuccessful in reducing the overpotential for the practical utilization of the eCO_2R technology. On the other hand, Pd is a promising catalyst, which could be used to convert CO_2 into $HCOO^-$ with high FE (>95%) at low overpotential (<0.2 V). However, the primary issue of using Pd as the electrocatalyst is its surface susceptibility to CO poisoning and high material cost. Different strategies, such as synthesizing Pd-based bimetallic alloys or core-shell nanoparticles, can be applied to improve the stability of Pd-based catalyst and reduce its material cost. Once the stability is improved, the performance of Pd-based catalysts should be tested inside a GDE for the continuous production of formate.

2. *eCO_2R into C_2 compounds*: Studies have demonstrated the capability of alkaline electrolytes to promote the C-C coupling reaction, reduce the overpotential and increase the selectivity toward C_2 compounds. Since CO is stable in a high pH environment, the two-step CO_2 reduction should be applied to produce C_2 compounds, instead of the direct conversion of CO_2. Although it has been demonstrated that C_2 compounds could be produced with a high partial current density using GDEs, the problems of low product selectivity and catastrophic water flooding of the GDE channels still need to be solved.

Once the technical challenges are successfully solved, the eCO_2R reaction could be the promising solution to close the carbon cycle and control the release of CO_2 and curb its concentration in the atmosphere.

ACKNOWLEDGEMENTS

The authors acknowledge the O.H. Reaugh Laboratory at Washington State University for its financial support.

REFERENCES

1. R. Lindsey, National Oceanic and Atmospheric Administration (2020).
2. D. Lüthi, M. Le Floch, B. Bereiter, T. Blunier, J.-M. Barnola, U. Siegenthaler, D. Raynaud, J. Jouzel, H. Fischer, K. Kawamura and T. F. Stocker, *Nature*, **453**, 379 (2008).
3. E. S. Blake and D. A. Zelinsky, National Oceanic and Atmospheric Administration and National Weather Service (2018).
4. J. D. Murphy, National Oceanic and Atmospheric Administration (2018).
5. J. P. Cangialosi, A. S. Latto and R. Berg, National Oceanic and Atmospheric Administration and National Weather Service (2018).
6. R. J. Pasch, A. B. Penny and R. Berg, National Oceanic and Atmospheric Administration and National Weather Service (2019).
7. Flooded future: Global vulnerability to sea level rise worse than previously understood. Climate Central (2019).
8. C40 Cities, 2019. https://www.c40.org/other/the-future-we-don-t-want-staying-afloat-the-urban-response-to-sea-level-rise.
9. P. A. Marchioro Ystad, O. Bolland and M. Hillestad, *Energy Procedia*, **23**, 33 (2012).
10. N. Dave, T. Do, D. Palyman, P. H. M. Feron, S. Xu, S. Gao and L. Liu, *Energy Procedia*, **4**, 1869 (2011).
11. M. McCann, D. Phan, X. Wang, W. Conway, R. Burns, M. Attalla, G. Puxty and M. Maeder, *J. Phys. Chem. A*, **113**, 5022 (2019).
12. M. Caplow, *J. Am. Chem. Soc.*, **90**, 6795 (1968).
13. P. V. Danckwerts, *Chem. Eng. Sci.*, **4**, 443 (1979).
14. F. Rezazadeh, W. F. Gale, G. T. Rochelle and D. Sachde, *Int. J. Greenhouse Gas Control*, **58**, 246 (2017).
15. M. Karimi, M. Hillestad and H. F. Svendsen, *Energy Procedia*, **23**, 15 (2012).
16. M. Bert, O. Davidson; H. de Coninck, M. Loos and L. Meyer, Cambridge University Press (2005).
17. M. A. Celia, J. M. Nordbotten, S. Bachu, M. Dobossy and B. Court, *Energy Procedia*, **1**, 2573 (2009).
18. J. Song and D. Zhang, *Environ. Sci. Technol.*, **47**, 9 (2013).
19. P. Kaiser, R. B. Unde, C. Kern and A. Jess, *Chem. Ing. Tech.*, **4**, 489 (2013).
20. F. Fisher and H. Tropsch, *Brennstoff-Chem*, **4**, 276 (1923).
21. R. B. Anderson, *Catalysts for the Fischer-Tropsch synthesis: Chap. 2 in catalysis*, Reinhold Publishing Corp, New York (1956).
22. C. Vayenas, *Modern aspects of electrochemistry*, Springer, New York (2008).
23. K. P. Kuhl, E. R. Cave, D. N. Abram and T. F. Jaramillo, *Energy Environ. Sci.*, **5**, 7050 (2012).
24. X. Min and M. W. Kanan, *J. Am. Chem. Soc.*, **137**, 4701 (2015).
25. R. H. Guo, C. F. Liu, T. C. Wei and C. C. Hu, *Electrochem. Commun.*, **80**, 24 (2017).
26. M. Valenti, N. P. Prasad, R. Kas, D. Bohra, M. Ma, V. Balasubramanian, L. Chu, S. Gimenez, J. Bisquert, B. Dam and W. A. Smith, *ACS Catal.*, **9**, 3527 (2019).
27. M. Jouny, W. Luc and F. Jiao, *Ind. Eng. Chem. Res.*, **57**, 2165 (2018).
28. D. W. Keith, G. Holmes, D. S. Angelo and K. A. Heidel, *Joule*, **2**, 1573 (2018).

29. M. Bolinger, J. Seel and R. Dana, Utility-Scale Solar, Empirical Trends in Project Technology, Cost, Performance, and PPA Pricing in the United States – 2019 Edition. Lawrence Berkeley National Laboratory (2019).
30. B. A. Rosen, A. Salehi-Khojin, M. R. Thorson, W. Zhu, D. T. Whipple, P. J. A. Kenis and R. I. Masel, *Science*, **334**, 643 (2011).
31. K. Manthiram, B. J. Beberwyck and A. P. Alivisatos, *J. Am. Chem. Soc.*, **136**, 13319 (2014).
32. D. Ren, B. S. Ang and B. S. Yeo, *ACS Catal.*, **6**, 8239 (2016).
33. C. T. Dinh, T. Burdyny, M. G. Kibria, A. Seifitokaldani, C. M. Gabardo, F. Pelayo García de Arquer, A. Kiani, J. P. Edwards, P. D. Luna, O. S. Bushuyev, C. Zou, R. Quintero-Bermudez, Y. Pang, D. Sinton and E. H. Sargent, *Science*, **360**, 783 (2018).
34. Industry - Ethylene and Other Olefins. Dialogue on European Decarbonisation Strategies.
35. B. A. Zhang, T. Ozel, J. S. Elias, C. Costentin and D. G. Nocera, *ACS Cent. Sci.*, **5**, 1097 (2019).
36. M. R. Singh, E. L. Clarkab and A. T. Bell, *Phys. Chem. Chem. Phys.*, **17**, 18924 (2015).
37. L. C. Weng, A. T. Bell and A. Z. Weber, *Phys. Chem. Chem. Phys.*, **20**, 16973 (2018).
38. A. Löwe, C. Rieg, T. Hierlemann, N. Salas, D. Kopljar, N. Wagner and I. E. Klemm, *ChemElectroChem*, **6**, 4497 (2019).
39. Z. Xing, L. Hu, D. S. Ripatti, X. Hu and X. Feng, *Nat. Commun.*, **136**, 1 (2021).
40. M. Azuma, K. Hashimoto, M. Watanabe and T. Sakata, *J. Electrochem. Soc.*, **137**, 1172 (1990).
41. R. Hegner, L. F. M. Rosa and F. Harnisch, *Appl. Catal., B*, **238**, 546 (2018).
42. B. Bohlen, D. Wastl, J. Radomski, V. Sieber and L. Vieir, *Electrochem. Commun.*, **110**, 106597 (2020).
43. B. Innocent, D. Liaigre, D. Pasquier, F. Ropital, J. M. Leger and K. B. Kokoh, *J. Appl. Electrochem.*, **39**, 227 (2009).
44. W. Lv, R. Zhang, P. Gao and L. Lei, *J. Power Sources*, **253**, 276 (2014).
45. E. Bertin, S. Garbarino, C. Roy, S. Kazemi and D. Guay, *J. CO_2 Util.*, **19**, 276 (2017).
46. Y. Hori, H. Wakebe, T. Tsukamoto and O. Koga, *Electrochim. Acta*, **39**, 1833 (1994).
47. J. T. Feaster, C. Shi, E. R. Cave, T. Hatsukade, D. N. Abram, K. P. Kuhl, C. Hahn, J. K. Nørskov and T. F. Jaramillo, *ACS Catal.*, **7**, 4822 (2017).
48. T. S. Safaei, A. Mepham, X. Zheng, Y. Pang, C. T. Dinh, M. Liu, D. Sinton, S. O. Kelley and E. H. Sargent, *Nano Lett.*, **16**, 7224 (2016).
49. N. Han, Y. Wang, H. Yang, J. Deng, J. Wu, Y. Li and Y. Li, *Nat. Commun.*, **9**, 1320 (2018).
50. W. Chen, J. Ji, X. Feng, X. Duan, G. Qian, P. Li, X. Zhou, D. Chen and W. Yuan, *J. Am. Chem. Soc.*, **136**, 167369 (2014).
51. F. J. Perez-Alonso, D. N. McCarthy, A. Nierhoff, P. Hernandez-Fernandez, C. Strebel, I. E. L. Stephens, J. H. Nielsen and I. Chorkendorff, *Angew. Chem.*, **51**, 4641 (2012).
52. B. Ávila-Bolívar, L. García-Cruz, V. Montiel and J. Solla-Gullón, *Molecules*, **24**, 2032 (2019).
53. W. Luo, W. Xie, M. Li, J. Zhang and A. Züttel, *J. Mater. Chem. A*, **7**, 4505 (2019).
54. Y. Qiu, J. Du, C. Dai, W. Dong and C. Tao, *J. Electrochem. Soc.*, **165**, 594 (2018).
55. A. D. Castillo, M. Alvarez-Guerra and A. Irabien, *AIChE J.*, **60**, 3557 (2014).
56. A. D. Castillo, M. Alvarez-Guerra, J. Solla-Gullón, A, Sáez, V. Montiel and A. Irabien, *Appl. Energy*, **157**, 165 (2015).
57. A. D. Castillo, M. Alvarez-Guerra, J. Solla-Gullón, A. Sáez, V. Montiel and A. Irabien, *J. CO_2 Util.*, **18**, 222 (2017).
58. W. Lee, Y. E. Kim, M. H. Youn, S. K. Jeong and K. T. Park, *Angew. Chem., Int. Ed.*, **57**, 6883 (2018).
59. B. I. Podlovchenko, E. A. Kolyadko and S. Lu, *J. Electroanal. Chem.*, **373**, 185 (1994).
60. C. Gabrielli, P. P. Grand, A. Lasia and H. Perrota, *J. Electrochem. Soc.*, **115**, 1937 (2016).
61. C. W. Lee, N. H. Cho, K. T. Nam, Y. J. Hwang and B. K. Min, *Nat. Commun.*, **10**, 3919 (2019).
62. B. Hammer and J. K. Nørskov, *Adv. Catal.*, **45**, 71 (2000).
63. R. Kortlever, I. Peters, S. Koper and M. T. M. Koper, *ACS Catal.*, **5**, 3916 (2015).
64. B. Jiang, X. G. Zhang, K. Jiang, D. Y. Wu and W. B. Cai, *J. Am. Chem. Soc.*, **140**, 2880 (2018).
65. W. J. Wang, S. Hwang, T. Kim, S. Ha and L. Scudiero, *Electrochim. Acta*, **387**, 138531 (2021).
66. R. Kortlever, J. Shen, K. J. P. Schouten, F. Calle-Vallejo and M. T. M. Koper, *J. Phys. Chem. Lett.*, **6**, 4073 (2015).
67. A. A. Peterson, F. Abild-Pedersen, F. Studt, J. Rossmeisl and J. K. Nørskov, *Energy Environ. Sci.*, **3**, 1311 (2010).
68. K. J. P. Schoute, Y. Kwo, C. J. M. van der Ham, H. Z. Qin and M. T. M. Koper, *Chem. Sci. J.*, **2**, 1902 (2011).
69. Y. Hori, A. Murata and R. Takahashi, *J. Chem. Soc., Faraday Trans. 1*, **85**, 2309 (1989).
70. A. Bagger, W. Ju, A. S. Varela, P. Strasser and J. Rossmeisl, *ChemPhysChem*, **18**, 3266 (2017).
71. T. Cheng, H. Xiao and W. A. Goddard III, *J. Phys. Chem. Lett.*, **6**, 4767 (2015).
72. Y. Lum, T. Cheng, W. A. Goddard III and J. W. Ager, *J. Am. Chem. Soc.*, **140**, 9337 (2018).
73. D. Raciti, M. Mao, J. H. Park and C. Wang, *J. Electrochem. Soc.*, **10**, 799 (2018).
74. H. Xiao, T. Cheng, W. A. Goddard III and R. Sundararaman, *J. Am. Chem. Soc.*, **138**, 483 (2016).
75. X. Liu, P. Schlexer, J. Xiao, Y. Ji, L. Wang, R. B. Sandberg, M. Tang, K. S. Brown, H. Peng, S. Ringe, C. Hahn, T. F. Jaramillo, J. K. Nørskov and K. Chan, *Nat. Commun.*, **10**, 32 (2019).
76. S. Verma, Y. Hamasaki, C. Kim, W. Huang, S. Lu, H. R. Molly Jhong, A. A. Gewirth, T. Fujigaya, N. Nakashima and P. J. A. Kenis, *ACS Energy Lett.*, **3**, 193 (2018).
77. M. E. Leonard, L. E. Clarke, A. Forner-Cuenca, S. M. Brown and F. R. Brushett, *ChemSusChem*, **13**, 400 (2020).
78. D. W. DeWulf, T. Jin and A. J. Bard, *J. Electrochem. Soc.*, **136**, 1686 (1989).
79. Y. Hori, R. Takahashi, Y. Yoshinami and A. Murata, *J. Phys. Chem. B*, **101**, 7075 (1997).
80. Z. Liu, R. I. Masel, Q. Chen, R. Kutz, H. Yang, K. Lewinski, M. Kaplun, S. Luopa and D. R. Lutz, *J. CO_2 Util.*, **15**, 50 (2016).
81. R. B. Kutz, Q. Chen, H. Yang, S. D. Sajjad, Z. Liu and R. I. Masel, *Energy Technol.*, **5**, 929 (2017).

82. T. Zheng, K. Jiang, N. Ta, Y. Hu, J. Zeng, J. Liu and H. Wang, *Joule*, **3**, 265 (2019).
83. Z. Yin, H. Peng, X. Wei, H. Zhou, J. Gong, M. Huai, L. Xiao, G. Wang, J. Lu and L. Zhuang, *Energy Environ. Sci.*, **12**, 2455 (2019).
84. L. Han, W. Zhou and C. Xiang, *Energy Lett.*, **3**, 855 (2018).
85. M. Jouny, W. Luc and F. Jiao, *Nat. Catal*, **1**, 748 (2018).
86. W. Luc, X. Fu, J. Shi, J. J. Lv, M. Jouny, B. H. Ko, Y. Xu, Q. Tu, X. Hu, J. Wu, Q. Yue, Y. Liu, F. Jiao and Y. Kang, *Nat. Catal*, **2**, 423 (2019).

Louis Scudiero obtained his B.S. and M.S. degrees in Physics in 1993 and 1995 from Washington State University where in 2002 he received his Ph.D. degree in Materials Science. He joined Washington State University in 2003 where he is currently a career track professor in the department of Chemistry and in the Materials Science and Engineering Program. His field of expertise is material characterization using spectroscopic and microscopic techniques. He has published in diverse research areas from developing materials for solar cells, air filtering, Li-ion batteries and fuel cells. His research is currently focused on nanomaterials for alternative energy such as electrochemical CO_2 reduction, direct formic acid and hydrogen fuel cells.

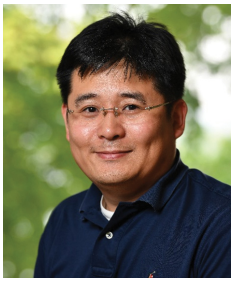

Su Ha obtained B.S. degree in Chemical Engineering from the North Carolina State University in 2000. He received M.S. and Ph.D. degrees in Chemical Engineering from the University of Illinois at Urbana-Champaign. He joined Washington State University in 2005 and is currently a professor in the Gene and Linda Voiland School of Chemical Engineering and Bioengineering at Washington State University. He is also a director for its O.H. Reaugh Laboratory for Oil and Gas Processing Research. He has published over 70 publications in the research areas of energy generations from alternative fuels. His researches have been cited over 5,500 times with an h-index of 30. In 2014, he was named as Highly Cited Researcher by Thomson Reuters.